Available online at www.sciencedirect.com
ScienceDirect
Trans. Nonferrous Met. Soc. China 31(2021) 878−886
Transactions of Nonferrous Metals Society of China
www.tnmsc.cn

Preparation and properties of graphene nanoplatelets reinforced aluminum composites

Zhong ZHENG[1], Xiao-xia YANG[2], Jian-chao LI[1], Xue-xi ZHANG [1], Imran MUHAMMAD[1,3], Lin GENG[1]

1. School of Materials Science and Engineering, Harbin Institute of Technology, Harbin 150001, China;
2. College of Materials Science and Engineering, Shandong University, Jinan 250014, China;
3. Mechanical Engineering Department, University of Engineering & Technology Taxila, Taxila 47050, Pakistan

Received 23 May 2020; accepted 28 December 2020

Abstract: 5.0 vol.% graphene nanoplatelets (GNPs) and aluminum powders were mixed to prepare GNPs/Al composites via high-energy ball milling (HEBM). The mixed powders were subjected to spark plasma sintering (SPS) and subsequent hot extrusion. The microstructure and mechanical properties of extruded composites were investigated by X-ray photoelectron spectroscopy (XPS), transmission electron microscopy (TEM) and tensile tests. In the extruded composites, 5.0 vol.% GNPs were dispersed homogeneously and no serious GNP−Al interfacial reaction occurred. As a result, the yield strength and ultimate tensile strength of the extruded GNPs/Al composites reached 462 and 479 MPa, which were 62% and 60% higher than those of the extruded Al matrix, respectively. The enhanced mechanical properties were attributed to the effective load transfer capacity of dispersed GNPs. This demonstrated that it may be promising to introduce dispersed high-content GNPs via HEBM, SPS and hot extrusion techniques and GNP−Al interfacial reaction can be controlled.

Key words: aluminum matrix composites; graphene nano-platelets; powder metallurgy; interface; microstructure; mechanical properties

1 Introduction

As a kind of high-performance reinforcement, graphene has been applied successfully to aluminum matrix composites (AMCs) [1−4]. From Refs. [5−31], it can be seen that the hardness, yield strength (YS) and ultimate tensile strength (UTS) of AMCs with 0.06−6.7 vol.% graphene exhibited an increment of 13%−71% [5,6,9,16,18], 14%−85% [8,11−13,15,17,19−21,25,27−31] and 9%−114% [7,8,10−15,17,20−31], respectively, compared with those of samples without graphene reinforcement. Since graphene-reinforced AMCs were reported in 2011, the interfacial reaction between graphene and Al has been found to be an important factor that hindered the improvement of graphene/Al composites' properties [5,32].

Up to now, a majority of graphene/Al composites have been produced by powder metallurgy (PM). LI et al [15] developed oxide graphene (GO)/Al composites with nano-laminate architecture via a flake assemble technique. They found that the elastic modulus and UTS of GO/Al composites were 21% and 50% higher than those of monolithic Al matrix, respectively. Although PM technique was proved to be effective in eliminating graphene aggregates in Al matrix, it may lead to unfavorable damage of graphene and formation of Al_4C_3 phase [33,34], which has detrimental effects on the mechanical properties of graphene/Al composites due to its brittle nature. Al_4C_3 was prone to be formed at high temperature for a prolonged time (e.g., casting [35] and 3D printing [36]). So, the

Corresponding author: Xue-xi ZHANG; Tel: +86-451-86415894; Fax: 86-451-86413921; E-mail: xxzhang@hit.edu.cn
DOI: 10.1016/S1003-6326(21)65546-2

graphene/Al interfacial reaction should be well controlled by low temperature casting [26] or cryo-milling followed by hot extrusion [13]. Thus, low-temperature, short-time hot working like spark plasma sintering (SPS) may hinder the formation of Al_4C_3 [30]. For example, no Al_4C_3 was formed in graphene/Al composites prepared by sintering at temperatures of 823−873 K [6,23]. In the graphene/Al composites prepared by wet mixing and sintering [17], the UTS reached the peak value at a graphene content of 0.4 vol.%. For composites prepared by wet mixing [6] and flake assembly [37] techniques, such critical graphene content may be 2.0 vol.%.

Flake powder metallurgy via ball milling is a feasible strategy to improve the strength of graphene/Al composites [38]. In this process, a high specific surface area of Al flakes is necessary to accommodate the graphene. Our recent work has demonstrated that 1.0 vol.% GNPs may be effectively attached on Al flake surface induced by the shear stress during ball milling (200 r/min for 5 h) [27]. However, even higher content of GNPs, e.g. 5.0 vol.%, cannot be homogeneously dispersed with Al flakes under low-energy ball milling (LEBM) conditions. Here, 5.0 vol.% GNPs were dispersed with Al powders via high-energy ball milling (HEBM, 300 r/min for 10 h). The mixed powders were then subjected to sintering by SPS and extrusion with a high extrusion ratio 25:1. The produced composites exhibited enhanced mechanical properties due to the homogeneous distribution of GNPs, demonstrating a promising method for fabricating high-content GNPs/Al composites.

2 Experimental

Al powder (purity ≥99.99%) with an average diameter of ~10 μm was supplied by Tianjiu Changsha Technology Company, China. The as-received GNPs (purity ≥99.9%) with an average thickness of 5−10 nm were supplied by Jicang Nano Technology Company, China. The Al powders were mixed with as-received GNPs in a planetary ball mill for 10 h at 300 r/min with ball to material mass ratio of 16:1. In our works, ball milling speeds of 100 r/min [33] and 200 r/min [27] were defined as LEBM or low-speed ball milling (LSBM). Here, a higher ball milling speed (300 r/min) is considered HEBM. The HEBM process was performed with 0.5 wt.% stearic acid as process control agent in argon atmosphere. The milled powders were placed into a graphite mold and subjected to sintering at a temperature of 723 K for 5 min to remove the stearic acid and then the green ingots were fabricated under a uniaxial pressure of 50 MPa in an HP-D250−1 SPS machine. The sintered ingot was heated to 723 K, kept at this temperature for 30 min and extruded into a rod with an extrusion ratio of 25:1. Graphite was used as the lubricant to reduce friction between sintered ingot and extrusion mold. For comparison, Al matrix was prepared at the same parameters.

Determined by Archimedes method, the relative densities of sintered Al matrix and composites are >99%. The morphology of mixed powders and microstructures of composites were observed by Zeiss field emission SEM Merlin Compact. Raman spectra tracking the structural integrity of GNPs in blended powders were acquired using a Renishaw inVia Reflex Raman confocal microscope (Gloucestershire, UK). X-ray photoelectron spectroscopy (XPS) measurement was performed using ESCLAB 250Xi equipped with a monochromator aluminum source. A Talos F200X TEM was used to investigate the morphology of GNPs and GNPs/Al composites. The samples for TEM analysis were prepared by ion thinning. Dog-bone shaped samples cut along the extrusion direction were used for tensile tests on a universal testing machine (Instron−5569).

3 Results and discussion

3.1 Graphene/Al interfacial reaction

For graphene/Al interfacial reaction, the relationship between Gibbs free energy change (ΔG_T) and temperature (T) can be described by $\Delta G_T=A+BT$, where A and B are temperature independent constants [39]. The obtained ΔG_T is far less than zero at temperatures of 700−900 K (Fig. 1), implying that Al may react with graphene to form Al_4C_3. The thickness of reaction layer Z and time t can be given by $Z=k\sqrt{t}$, where the theoretical kinetic diffusion coefficient (k) can be expressed by Arrhenius formula [40,41]. The empirical expression of k and T may be expressed by $k=k_0\exp[-Q/(RT)]$ (Fig. 1). Apparently, k is almost zero at below 823 K and increases exponentially with the increase of T.

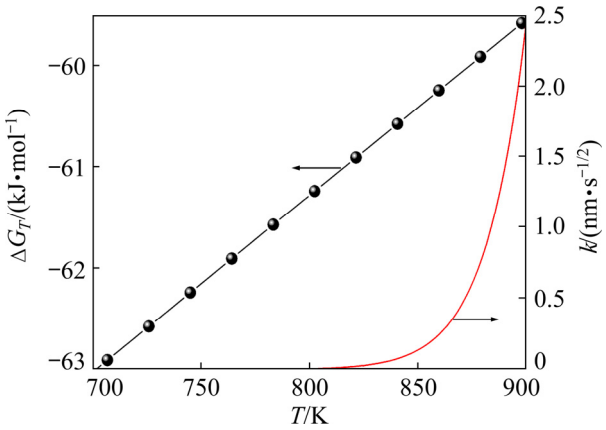

Fig. 1 Thermodynamic and kinetic curves for reaction between graphene and Al

3.2 Microstructure of GNPs/Al composites

Figure 2(a) shows the morphology of 5.0 vol.% GNPs/Al composites produced by HEBM. Distributions of the diameters of Al particles and lateral sizes of GNPs were determined using Image Pro Plus software, as plotted in Figs. 2(b) and (c), respectively. It can be seen that the average diameter of Al particles produced by HEBM is 110 μm, which is larger than that of the as-received Al powders, implying the occurrence of cold-welding during ball milling. On the other hand, GNP slices (inset in Fig. 2(a)) attached on the surface of Al particles were observed. The average lateral size of GNP slice is 0.20 μm, which is one eighth of as-received GNPs (~1.5 μm in lateral size). The reduction in GNP lateral size may be attributed to the shear stress induced by HEBM.

The Raman spectra of GNPs/Al composites and as-received GNPs are shown in Fig. 3. One strong broad peak centered at 1343 cm^{-1} corresponds to D band (disordered defect structure) and that centered at 1575 cm^{-1} corresponding to G band (ordered graphene structure) [42]. Generally speaking, the intensity ratio of D-band to G-band (I_D/I_G) represents defect density or disorder degree in graphene. The I_D/I_G value increased from 0.1:1 in as-received GNPs to 1.4:1 in GNPs/Al composites, implying the increase of defect density in GNPs induced by HEBM. At the same time, the I_D/I_G value of GNPs/Al composites by HEBM (300 r/min for 10 h) is similar to that of LEBM (150 r/min for 1.5 h [43]), indicating that embedding of GNPs in Al particles may protect GNPs from serious damage.

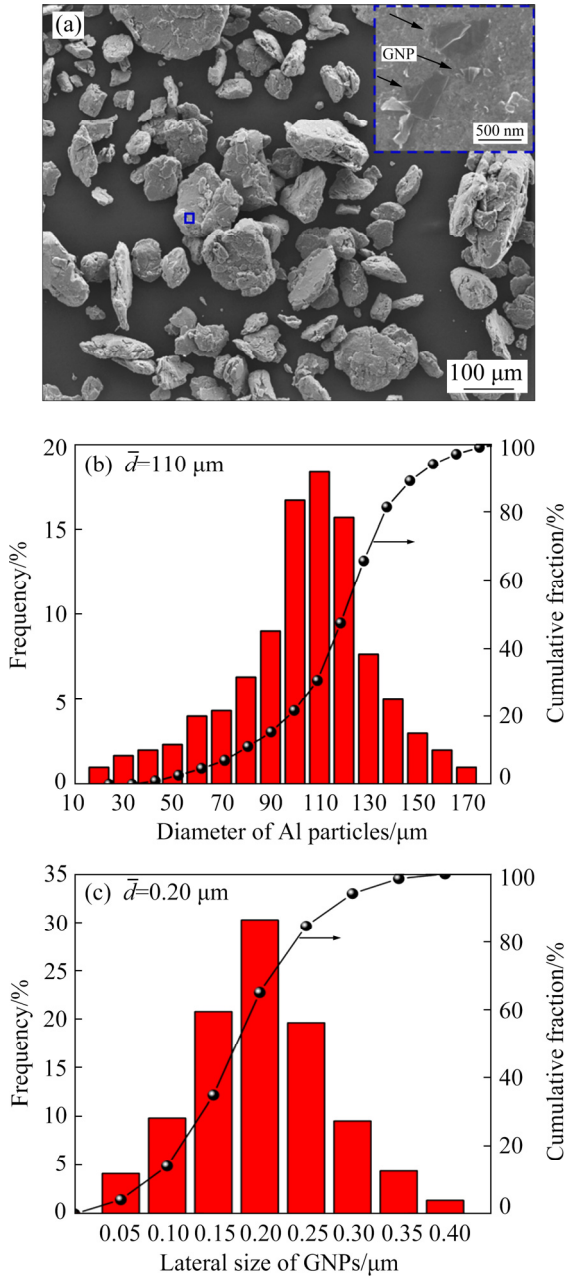

Fig. 2 Morphology and size of 5.0 vol.% GNPs/Al composites produced by HEBM: (a) SEM image showing morphology of mixed powders (The inset shows GNP slices on the surface of Al particles); (b) Diameter distribution of Al particles; (c) Lateral size distribution of GNP slices

While SPS at higher temperature is helpful for the densification of composites, graphene and Al are prone to react at such high temperatures [22,36]. As the value of k is very small at 723 K (Fig. 1), interfacial reaction between graphene and Al is possibly not serious. In order to reveal the interfacial reaction state, XPS spectra were obtained, as shown in Fig. 4. The peaks centered at 743 and

284.5 eV correspond to Al and C, respectively. High resolution Al 2p and C 1s XPS spectra of sintered GNPs/Al composites are shown in Figs. 4(a) and (b), respectively. No peaks at 72.7 and 282.2 eV, corresponding to Al_4C_3 phase [36], were observed, implying that the interfacial reaction between GNPs and Al may be too weak to be detectable via XPS.

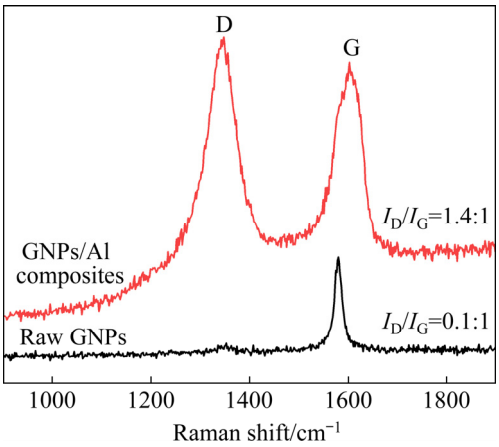

Fig. 3 Raman spectra of 5.0 vol.% GNPs/Al composites and as-received GNPs

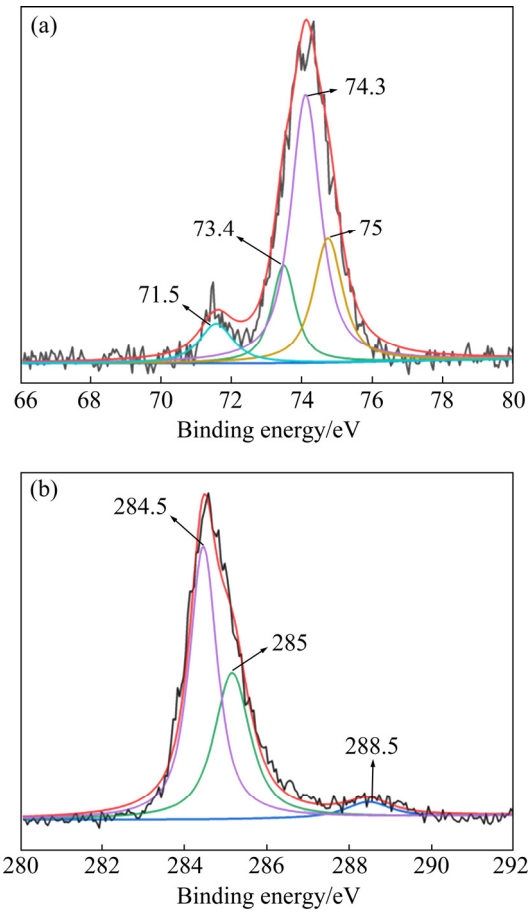

Fig. 4 XPS spectra of sintered 5.0 vol.% GNPs/Al composites: (a) Al 2p; (b) C 1s

Figure 5(a) shows the GNPs distribution state in the extruded 5.0 vol.% GNPs/Al composites. HRTEM image (inset in Fig. 5(a)) shows that the lattice fringe has a spacing of ~0.34 nm, corresponding to the interplanar spacing of graphite (0002) [44]. GNPs are dispersed homogeneously in extruded composites (Fig. 5(c)), which is favorable for improving mechanical properties of the composites [45]. Nano-sized grains are formed in extruded composites and Al matrix (Figs. 5(b) and (d)). Compared with the average grain size of Al matrix (279 nm), the grain size of composite is reduced to 196 nm, indicating that addition of GNPs is favorable for grain refinement [46]. This may be related to the presence of GNPs at Al grain boundaries, which reduced the mobility of Al grain boundaries during high temperature dwelling and deformation processes [33].

3.3 Mechanical properties and fracture behaviors

The YS, UTS and fracture elongation are summarized in Table 1. The YS of composites (~462 MPa) is 1.6 times as high as that of Al matrix (~286 MPa), which is the outcome of well-dispersed GNPs and fine Al grains in the composites (Fig. 5). Furthermore, the UTS of composites reaches ~479 MPa, which is comparable or even higher than that of many graphene/Al composites with lower or similar GNP contents [8,10,11,13,17,18,20−24,26−28,30,47]. However, the fracture elongation of the composite is ~2.7%, which is much smaller than that of Al matrix (~10.9%). This may be related to the damage of GNPs after HEBM (I_D/I_G value increased from 0.1:1 for the as-received GNPs to 1.4:1 for GNPs/Al composites, see Fig. 3). This shows that, in order to enhance the strength and plasticity of GNPs/Al composites, it is necessary to achieve homogeneous distribution of GNPs without damage GNPs structure.

The fracture surface morphology of 5.0 vol.% GNPs/Al composites is displayed in Fig. 6. It can be seen that dimples and GNP slices exist on the fracture surfaces of composites. It is also noted that GNPs (marked circles in Fig. 6(b)) may bridge cracks, leading to the crack propagation resistance for composite. Therefore, the dispersed GNPs exhibit significant load transfer strengthening effect; thus, mechanical properties of the composites were improved.

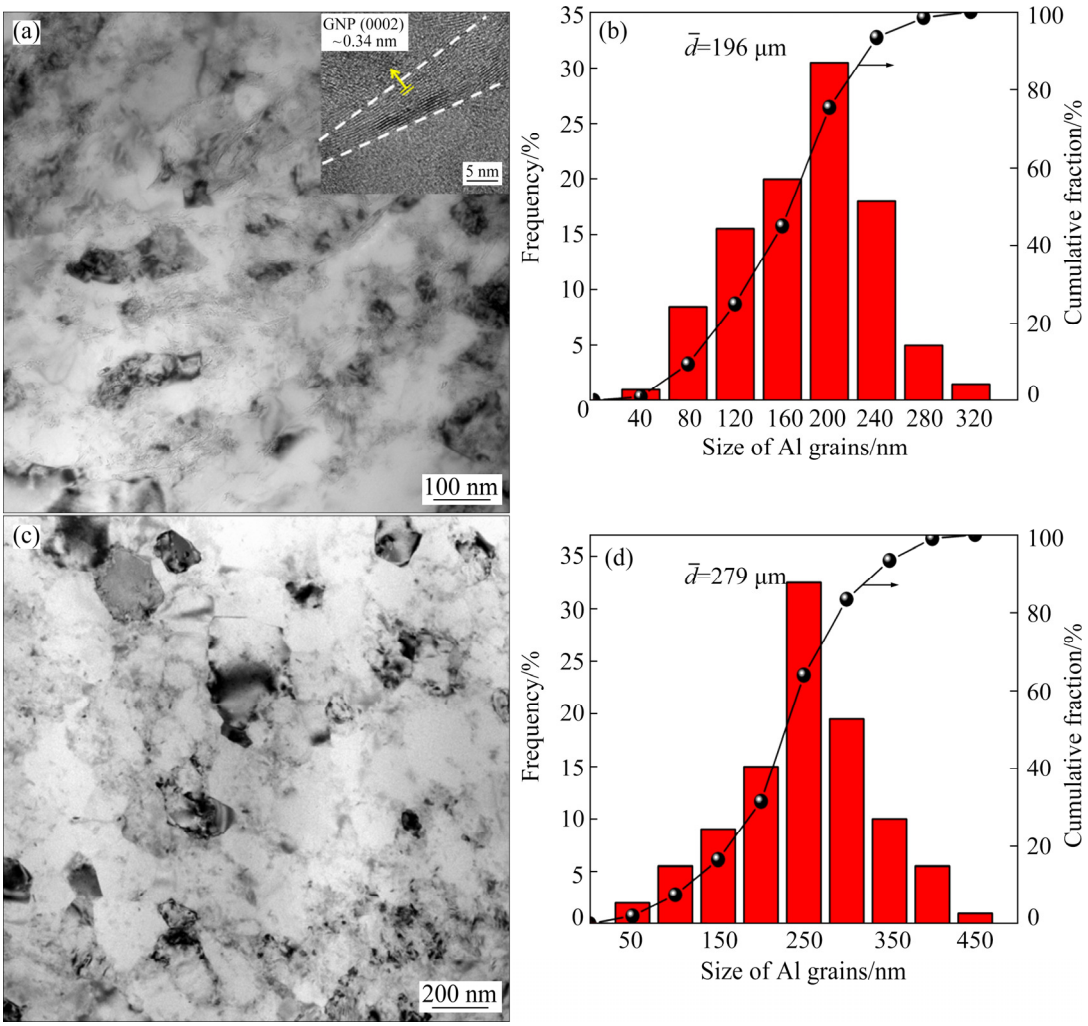

Fig. 5 TEM images and Al grain size of extruded 5.0 vol.% GNPs/Al composite and Al matrix: (a) TEM micrograph showing GNPs and Al grains (The inset shows HRTEM image of GNPs); (b) Statistical Al grain size in composites; (c) TEM micrograph showing Al grains in Al matrix; (d) Statistical size of Al grain size in Al matrix

Table 1 Yield strength (YS), ultimate tensile strength (UTS) and fracture elongation (δ) of extruded Al matrix and 5.0 vol.% GNPs/Al composites

Material	YS/MPa	UTS/MPa	δ/%
Al matrix	286±3	300±5	10.9±1
GNPs/Al composites	462±17	479±22	2.7±0.8

In order to reveal the reinforcing efficiency of GNPs, a normalized parameter $\Delta\sigma=\sigma_c-\sigma_m$, where σ_c and σ_m are UTS values of composites and Al matrix, respectively, is proposed. The UTS increment $\Delta\sigma$ of graphene/Al composites and their fracture elongations in open literatures are summarized in Fig. 7. The fabrication techniques and graphene contents in Refs. [7,8,10−13,15,20,22−28,37] are given in Table 2. Here, different $\Delta\sigma$ may be attributed to graphene dispersion state and graphene/Al interfacial reaction state by various fabrication techniques. Usually, graphene/Al composites possess significantly enhanced UTS owning to the uniform distribution of graphene in Al matrix by employing ball milling [12,24] or flake assemble [15,20] techniques. In addition, improving the distribution of graphene in Al matrix via secondary-processing techniques, such as rolling [12] and extrusion [13,24], exhibited higher UTS. From Fig. 7 and Table 1, it is also noticed that the UTS increment of the composite is linked inversely to its fracture elongation. Generally, graphene/Al composites show low fracture elongation owing to damage graphene structure [6] or serious interfacial reaction [11].

In this study, GNPs were embedded in cold-welded Al particles effectively, which protected GNPs from the serious damage during HEBM.

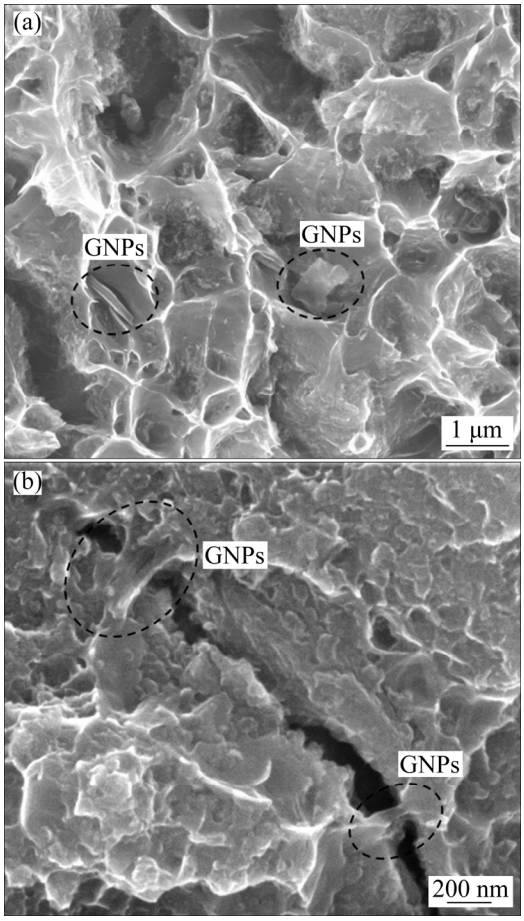

Fig. 6 SEM images showing fracture surfaces of extruded 5.0 vol.% GNPs/Al composites

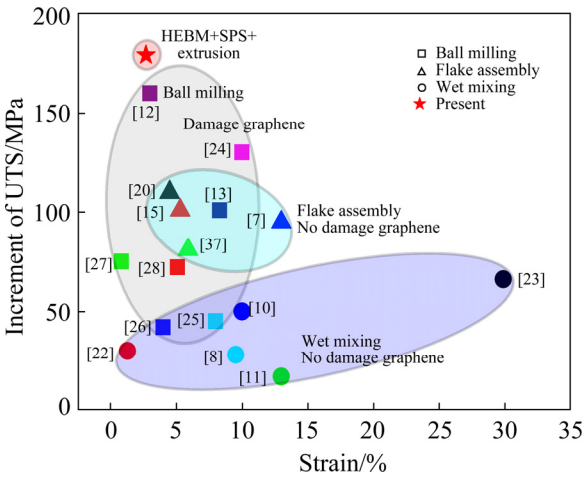

Fig. 7 Increment of ultimate tensile strength (UTS) in graphene/Al composites prepared by various fabricating techniques including wet mixing + spark plasma sintering [22,23]/hot extrusion [8,11]/high pressure torsion [10], flake assembly + hot rolling [15,20]/hot extrusion [7,37], ball milling + spark plasma sintering[28]/cold drawing [27]/hot rolling [26]/friction stir processing [25]/hot extrusion [13,24]/hot rolling [12]

Table 2 Al composites with different contents of graphene prepared by various fabricating techniques

Composite ingredient	Fabricating technique	Ref.
0.4 vol.% GO[d]/Al	Flake assembly + cold pressing + extrusion	[7]
0.4 vol.% GNP[c]/Al	Wet mixing + cold pressing + extrusion	[8]
0.27 vol.% GNP[c]/Al	Wet mixing + cold pressing + HPT [f]	[10]
1.3 vol.% GNP[c]/Al	Wet mixing + cold pressing + extrusion	[11]
2 vol.% GO[d]/Al	Flake assembly + hot pressing + extrusion	[37]
0.7 vol.% FLG[b]/Al	BM [e] + hot rolling	[12]
1.3 vol.% GNF[a]/Al	BM [e] + hot pressing + extrusion	[13]
2 vol.% GO[d]/Al	Flake assembly + hot pressing + hot rolling	[15]
0.2 vol.% GO[d]/Al	Self-assemble + hot pressing + hot rolling	[20]
1.3 vol.% GNP[c]/Al	Wet mixing + SPS [g]	[22]
0.67 vol.% GNP[c]/Al	Wet mixing + SPS [g]	[23]
0.7 vol.% GNP[c]/Al	BM [e] + cold pressing + infiltration + extrusion	[24]
1.3 vol.% GNP[c]/2009Al	BM [e] + hot pressing + FSP [h]	[25]
0.26 vol.% GNP[c]/Al	BM [e] + cold pressing + casting + hot rolling	[26]
1.0 vol.% GNP[c]/Al	BM [e] + extrusion + cold drawing	[27]
0.67 vol.% GNP[c]/Al	BM [e] + SPS [g]	[28]

[a] GNF — Graphene nanoflake; [b] FLG — Few-layered graphene; [c] GNP—Graphene nanoplatelet; [d] GO—Graphene oxide; [e] BM—Ball milling; [f] HPT—High pressure torsion; [g] SPS—Spark plasma sintering; [h] FSP—Friction stir processing

Subsequently, the mixed powders were sintered by SPS at a low temperature of 723 K in order to avoid unfavorable interfacial reaction. Meanwhile, the high shear strain produced during hot extrusion help for eliminating GNP dense zones and realizing homogeneous distribution of GNPs (Fig. 5). As a result, the UTS and YS of GNPs/Al composites reached as high as about 479 and 462 MPa, respectively (Table 1) because of high load transfer strengthening efficiency of GNPs.

4 Conclusions

(1) Homogeneous dispersion of high-content GNPs in Al matrix was achieved via cold-welding during HEBM. This was favorable for avoiding

serious damage of GNP structure during HEBM and preventing unfavorable interfacial reaction during SPS.

(2) The SPS and hot extrusion temperatures were determined to be 723 K. The hot extrusion induced homogeneous distribution of GNPs in composites, while the low sintering temperatures prevented interfacial reaction.

(3) The extruded 5.0 vol.% GNPs/Al composites had YS of ~462 MPa and UTS of ~479 MPa, which were 62% and 60% higher than those of Al matrix, respectively. The enhanced YS and UTS were attributed to well-dispersed GNPs and nano-grains in the extruded composites.

Acknowledgments

The authors are grateful for the financial supports from National Key R&D Program of China (2017YFB0703103), and Key Area R&D Program of Guangdong Province, China (2019B010942001)

References

[1] HUANG Yu, OUYANG Qiu-bao, ZHU Cheng-nan, ZHU Jing, ZHANG Guo-ding, ZHANG Di. Effect of alumina coating and extrusion deformation on microstructures and thermal properties of short carbon fiber Al composites [J]. Bulletin of Materials Science, 2018, 41: 21−32.

[2] SHARMA A, SHARMA V, PAUL J. A comparative study on microstructural evolution and surface properties of graphene/CNT reinforced Al6061−SiC hybrid surface composite fabricated via friction stir processing [J]. Transactions of Nonferrous Metals Society of China, 2019, 29: 2005−2026.

[3] ZHENG Zhong, ZHONG Shi-jiang, ZHANG Xue-xi, LI Jian-chao, GENG Lin. Graphene nano-platelets reinforced aluminum composites with anisotropic compressive properties [J]. Materials Science and Engineering A, 2020, 798: 140234.

[4] PANDEY N, CHAKRABARTY I, BARKANE K, MEHTA N S, MAJHI M R. Microstructure, mechanical and wear properties of aluminum borate whisker reinforced aluminum matrix composites [J]. Transactions of Nonferrous Metals Society of China, 2020, 30: 1731−1742.

[5] LATIEF F H, SHERIF S M, ALMAJID A A, JUNAEDI H. Fabrication of exfoliated graphite nanoplatelets-reinforced aluminum composites and evaluating their mechanical properties and corrosion behavior [J]. Journal of Analytical and Applied Pyrolysis, 2011, 92: 485−492.

[6] LATIEF F H, SHERIF S M. Effects of sintering temperature and graphite addition on the mechanical properties of aluminum [J]. Journal of Industrial and Engineering Chemistry, 2012, 18: 2129−2134.

[7] WANG Jing-yue, LI Zhi-qiang, FAN Gen-lian, PAN Huan-huan, CHEN Zhi-xin, ZHANG Di. Reinforcement with graphene nanosheets in aluminum matrix composites [J]. Scripta Materialia, 2012, 66: 594−597.

[8] RASHAD M, PAN Fu-sheng, TANG Ai-tao, ASIF M. Effect of graphene nanoplatelets addition on mechanical properties of pure aluminum using a semi-powder method [J]. Progress in Natural Science: Materials International, 2014, 24: 101−108.

[9] PÉREZ B R, BOLAÑOS M D, BONILLA M J, ESTRADA G I, MARTÍNEZ S R. Microstructural and hardness behavior of graphene-nanoplatelets/aluminum composites synthesized by mechanical alloying [J]. Journal of Alloys and Compounds, 2014, 615: s578−s582.

[10] ZHAO Li-yuan, LU Hui-min, GAO Zhi-jiang. Microstructure and mechanical properties of Al/graphene composite produced by high-pressure torsion [J]. Advanced Engineering Materials, 2015, 17: 976−981.

[11] RASHAD M, PAN Fu-sheng, YU Zheng-wen, ASIF M, LIN Han, PAN Rong-jian. Investigation on microstructural, mechanical and electrochemical properties of aluminum composites reinforced with graphene nanoplatelets [J]. Progress in Natural Science: Materials International, 2015, 25: 460−470.

[12] SHIN S E, CHOI H J, SHIN J H, BAE D H. Strengthening behavior of few-layered graphene/aluminum composites [J]. Carbon, 2015, 82: 143−151.

[13] LI J L, XIONG Y C, WANG X D, YAN S J, YANG C, HE W W, CHEN J Z, WANG S Q, ZHANG X Y, DAI S L. Microstructure and tensile properties of bulk nanostructured aluminum/graphene composites prepared via cryomilling [J]. Materials Science and Engineering A, 2015, 626: 400−405.

[14] SHIN S E, BAE D H. Deformation behavior of aluminum alloy matrix composites reinforced with few-layer graphene [J]. Composites (Part A): Applied Science and Manufacturing, 2015, 78: 42−47.

[15] LI Zan, GUO Qiang, LI Zhi-qiang, FAN Gen-lian, XIONG Ding-bang, SU Yi-shi, ZHANG Jie, ZHANG Di. Enhanced mechanical properties of graphene (reduced graphene oxide)/aluminum composites with a bioinspired nano-laminated structure [J]. Nano Letters, 2015, 15: 8077−8083.

[16] LIU J H, KHAN U, COLEMAN J, FERNANDEZ B, RODRIGUEZ P, NAHER S, BRABAZON D. Graphene oxide and graphene nanosheet reinforced aluminium matrix composites: Powder synthesis and prepared composite characteristics [J]. Materials & Design, 2016, 94: 87−94.

[17] GAO Xin, YUE Hong-yan, GUO Er-jun, ZHANG Hong, LIN Xuan-yu, YAO Long-hui, WANG Bao. Preparation and tensile properties of homogeneously dispersed graphene reinforced aluminum matrix composites [J]. Materials & Design, 2016, 94: 54−60.

[18] ASGHARZADEH H, SEDIGH M. Synthesis and mechanical properties of Al matrix composites reinforced with few-layer graphene and graphene oxide [J]. Journal of Alloys and Compounds, 2017, 728: 47−62.

[19] KWON H, MONDAL J, ALOGAB K A, SAMMELSELG V, TAKAMICHI M, KAWASKI A, LEPAROUX M. Graphene oxide-reinforced aluminum alloy matrix composite materials fabricated by powder metallurgy [J]. Journal of Alloys and Compounds, 2017, 698: 807−813.

[20] ZHAO Mei, XIONG Ding-bang, TAN Zhan-qiu, FAN Gen-lian, GUO Qiang, GUO Cui-ping, LI Zhi-qiang, ZHANG Di. Lateral size effect of graphene on mechanical properties of aluminum matrix nanolaminated composites [J]. Scripta Materialia, 2017, 139: 44−48.

[21] LI Gang, XIONG Bo-wen. Effects of graphene content on microstructures and tensile property of graphene-nanosheets/aluminum composites [J]. Journal of Alloys and Compounds, 2017, 697: 31−36.

[22] BISHT A, SRIVASTAVA M, KUMAR R M, LAHIRI I, LAHIRI D. Strengthening mechanism in graphene nanoplatelets reinforced aluminum composite fabricated through spark plasma sintering [J]. Materials Science and Engineering A, 2017, 695: 20−28.

[23] BHADAURIA A, SINGH L K, LAHA T. Effect of physio-chemically functionalized graphene nanoplatelet reinforcement on tensile properties of aluminum nanocomposite synthesized via spark plasma sintering [J]. Journal of Alloys and Compounds, 2018, 748: 783−793.

[24] YANG Wen-shu, ZHAO Qi-qi, XIN Ling, QIAO Jing, ZOU Jun-yu, SHAO Pu-zhen, YU Zhen-he, ZHANG Qiang, WU Gao-hui. Microstructure and mechanical properties of graphene nanoplates reinforced pure Al matrix composites prepared by pressure infiltration method [J]. Journal of Alloys and Compounds, 2018, 732: 748−758.

[25] ZHANG Z W, LIU Z Y, XIAO B L, NI D R, MA Z Y. High efficiency dispersal and strengthening of graphene reinforced aluminum alloy composites fabricated by powder metallurgy combined with friction stir processing [J]. Carbon, 2018, 135: 215−223.

[26] LI Min, GAO Hai-yan, LIANG Jia-miao, GU Sun-wang, YOU We-ren, SHU Da, WANG Jun, SUN Bao-de. Microstructure evolution and properties of graphene nanoplatelets reinforced aluminum matrix composites [J]. Materials Characterization, 2018, 140: 172−178.

[27] LI Jian-chao, ZHANG Xue-xi, GENG Lin. Improving graphene distribution and mechanical properties of GNP/Al composites by cold drawing [J]. Materials & Design, 2018, 144: 159−168.

[28] BHADAURIA A, SINGH L K, LAHA T. Combined strengthening effect of nanocrystalline matrix and graphene nanoplatelet reinforcement on the mechanical properties of spark plasma sintered aluminum based nanocomposites [J]. Materials Science and Engineering A, 2019, 749: 14−26.

[29] LI Jian-chao, ZHANG Xue-xi, GENG Lin. Effect of heat treatment on interfacial bonding and strengthening efficiency of graphene in GNP/Al composites [J]. Composites (Part A): Applied Science and Manufacturing, 2019, 121: 487−498.

[30] LI Min, ZHANG Zhen, GAO Hai-yan, WANG Yu-fei, LIANG Jia-miao, SHU Da, WANG Jun, SUN Bao-de. Formation of multilayer interfaces and the load transfer in graphene nanoplatelets reinforced Al matrix composites [J]. Materials Characterization, 2020, 159: 110018.

[31] ZHENG Zhong, ZHANG Xue-xi, LI Jian-chao, GENG Lin. Achieving homogeneous distribution of high-content graphene in aluminum alloys via high-temperature cumulative shear deformation [J]. Materials & Design, 2020, 193: 108796.

[32] BARTOLUCCI S F, PARAS J, RAFIEE M A, RAFIEE J, LEE S, KAPOOR D, KORATKAR N. Graphene−aluminum nanocomposites [J]. Materials Science and Engineering A, 2011, 528: 7933−7937.

[33] ZHENG Zhong, ZHANG Xue-xi, LI Jian-chao, GENG Lin. High-content graphene nanoplatelet reinforced aluminum composites produced by ball milling and hot extrusion [J]. Science China: Technological Sciences, 2020, 63: 1426−1435.

[34] MUKHERJEE B, KUMAR R, ISLAM A, RAHMAN S A, KESHRI A K. Evaluation of strength-ductility combination by in-situ tensile testing of graphene nanoplatelets reinforced shroud plasma sprayed nickel−aluminium coating [J]. Journal of Alloys and Compounds, 2018, 765: 1082−1089.

[35] YANG H N, GU M Y, JIANG W J, ZHANG G D. Interface microstructure and reaction in Gr/Al metal matrix composites [J]. Journal of Materials Science, 1996, 31: 1903−1907.

[36] HU Zeng-rong, CHEN Feng, XU Jia-le, NIAN Qiong, LIN Dong, CHEN Chang-jun, ZHU Xing, CHEN Yao, ZHANG Min. 3D printing graphene−aluminum nanocomposites [J]. Journal of Alloys and Compounds, 2018, 746: 269−276.

[37] LI Zan, FAN Gen-lian, GUO Qiang, LI Zhi-qiang, SU Yi-shi, ZHANG Di. Synergistic strengthening effect of graphene-carbon nanotube hybrid structure in aluminum matrix composites [J]. Carbon, 2015, 95: 419−427.

[38] JIANG Yuan-yuan, TAN Zhan-qiu, XU Run, FAN Gen-lian, XIONG Ding-bang, GUO Qiang, SU Yi-shi, LI Zhi-qiang, ZHANG Di. Tailoring the structure and mechanical properties of graphene nanosheet/aluminum composites by flake powder metallurgy via shift-speed ball milling [J]. Composites (Part A): Applied Science and Manufacturing, 2018, 111: 73−82.

[39] DENG Chun-feng, ZHANG Xue-xi, WANG De-zun. Chemical stability of carbon nanotubes in the 2024Al matrix [J]. Materials Letters, 2007, 61: 904−907.

[40] CAI Jun-meng, HE Fang, YI Wei-ming, YAO Fu-sheng. A new formula approximating the Arrhenius integral to perform the non-isothermal kinetics [J]. Chemical Engineering Journal, 2006, 124: 15−18.

[41] MASLOV M M, OPENOV L A, PODLIVAEV A I. On the Vineyard formula for the pre-exponential factor in the Arrhenius law [J]. Physics of the Solid State, 2014, 56: 1239−1244.

[42] HUANG Chen-yang, HU Shui-ping, CHEN Kai. Influence of rolling temperature on the interfaces and mechanical performance of graphene-reinforced aluminum−matrix composites [J]. International Journal of Minerals, Metallurgy, and Materials, 2019, 26: 752−759.

[43] FERRARI A C, ROBERTSON J. Interpretation of Raman spectra of disordered and amorphous carbon [J]. Physical Review B, 2000, 61: 14095−14107.

[44] JIANG Lin, LI Zhi-qiang, FAN Gen-lian, CAO Lin-lin, ZHANG Di. The use of flake powder metallurgy to produce carbon nanotube (CNT)/aluminum composites with a homogenous CNT distribution [J]. Carbon, 2012, 50: 1993−1998.

[45] XU Run, TAN Zhan-qiu, XIONG Ding-bang, FAN Gen-lian, GUO Qiang, ZHANG Jie, SU Yi-shi, LI Zhi-qiang, ZHANG Di. Balanced strength and ductility in CNT/Al composites

achieved by flake powder metallurgy via shift-speed ball milling [J]. Composites (Part A): Applied Science and Manufacturing, 2017, 96: 57−66.

[46] YAN Lai-peng, TAN Zhan-qiu, JI Gang, LI Zhi-qiang, FAN Gen-lian, SCHRYVERS D, SHAN Ai-dang, ZHANG Di. A quantitative method to characterize the Al_4C_3-formed interfacial reaction: The case study of MWCNT/Al composites [J]. Materials Characterization, 2016, 112: 213−218.

[47] CZEPPE T, KORINIKOVA G, OZGA P, LITYŃSKA-DOBRZYŃSKA L, SOCHA R. Application of the high pressure torsion supported by mechanical alloying for the metal-graphene composites preparation [J]. Mechanik, 2015, 88: 147−157.

石墨烯纳米片增强铝基复合材料的制备与性能

郑 忠[1]，杨晓霞[2]，李建超[1]，张学习[1]，Imran MUHAMMAD[1,3]，耿 林[1]

1. 哈尔滨工业大学 材料科学与工程学院，哈尔滨 150001；

2. 山东大学 材料科学与工程学院，济南 250014；

3. Mechanical Engineering Department, University of Engineering & Technology Taxila, Taxila 47050, Pakistan

摘 要：采用高能球磨、放电等离子烧结以及热挤压工艺制备含量为 5.0%(体积分数)的石墨烯增强铝基复合材料。分别采用 X 射线光电子能谱、透射电镜及拉伸试验研究挤压态复合材料的显微组织与力学性能，发现 5.0%(体积分数)的石墨烯分散在铝晶界上，并且未与铝基体发生界面反应。最终，挤压态复合材料的屈服强度和抗拉强度高达 462 MPa 和 479 MPa，分别比挤压态铝基体提高 62%和 60%。断口分析表明，在断裂过程中复合材料中分散的石墨烯起到明显的载荷传递的作用。上述结果表明，采用高能球磨、放电等离子烧结以及热挤压制备工艺可将高含量石墨烯分散于铝合金中，且能控制石墨烯和铝基体之间的界面反应。

关键词：铝基复合材料；石墨烯纳米片；粉末冶金；界面；显微组织；力学性能

(Edited by Wei-ping CHEN)